



Hydrogen-assisted fatigue crack growth: Pre-charging vs in-situ testing in gaseous environments

A. Zafra^a, G. Álvarez^{a,b}, G. Benoit^c, G. Henaff^c, E. Martínez-Pañeda^{a,*}, C. Rodríguez^b, J. Belzunce^b

^a Department of Civil and Environmental Engineering, Imperial College London, London, SW7 2AZ, UK

^b SIMUMECAMAT Research Group, University of Oviedo, Polytechnic School of Engineering of Gijón, East Building, 33203, Asturias, Spain

^c Institut Pprime UPR 3346, Ecole Nationale Supérieure de Mécanique et d'Aérotechnique (ISAE-ENSMA), Centre National de la Recherche Scientifique (CNRS), Université de Poitiers, 89073 CEDEX 9, 86000 Poitiers, France

ARTICLE INFO

Keywords:

Hydrogen embrittlement
Fatigue crack growth rate
Welds
H2 pre-charging
H2 in-situ testing

ABSTRACT

We investigate the implications of conducting hydrogen-assisted fatigue crack growth experiments in a hydrogen gas environment (in-situ hydrogen charging) or in air (following exposure to hydrogen gas). The study is conducted on welded 42CrMo4 steel, a primary candidate for the future hydrogen transport infrastructure, allowing us to additionally gain insight into the differences in behavior between the base steel and the coarse grain heat affected zone. The results reveal significant differences between the two testing approaches and the two weld regions. The differences are particularly remarkable for the comparison of testing methodologies, with fatigue crack growth rates being more than one order of magnitude higher over relevant loading regimes when the samples are tested in a hydrogen-containing environment, relative to the pre-charged samples. Aided by finite element modelling and microscopy analysis, these differences are discussed and rationalized. Independent of the testing approach, the heat affected zone showed a higher susceptibility to hydrogen embrittlement. Similar microstructural behavior is observed for both testing approaches, with the base metal exhibiting martensite lath decohesion while the heat affected zone experienced both martensite lath decohesion and intergranular fracture.

1. Introduction

The interest in understanding hydrogen-metal interactions is growing significantly due to the role that hydrogen is deemed to play in the energy transition. Owing to the relatively low volumetric energy density of hydrogen gas, a cost-effective hydrogen energy infrastructure requires operating with pressures on the order of 30–50 MPa [1]. Then, the main challenge lies in maintaining the structural integrity of storage and transport components, given that hydrogen can reduce the fracture toughness, failure strain and fatigue crack growth resistance of steels (by orders of magnitude), through a phenomenon often referred to as *hydrogen embrittlement* [2–6]. Since hydrogen embrittlement is strongly dependent on the material microstructure and strength, material selection plays an essential role in minimizing the risk of this phenomenon. Medium-strength quenched and tempered CrMo steels are primary candidates for hydrogen storage and transport as they are currently being used in hydrogen-containing environments in both petrochemical and nuclear industries [7–10]. Beyond material selection, the

fabrication process is also important when assessing hydrogen embrittlement in hydrogen infrastructure. The use of welding is widespread but, due to the high thermal inputs involved, it results in different microstructures being generated along the welded joint, giving rise to hardening/softening, grain coarsening, residual stresses, and local variations in the mechanical properties. Welding can also generate small imperfections such as cavities, pores, and cracks [11]. All of these microstructural changes should be carefully considered as hydrogen is especially harmful in hard microstructures, with a high density of structural defects [12–16]. Thus, there is a need to understand the microstructure-hydrogen susceptibility interplay in welded components and under technologically-relevant conditions (cyclic loading).

Experimentally, hydrogen is typically introduced in the material from a gaseous environment or electrochemically from an aqueous hydrogen-rich solution [17–20]. The latter approach has traditionally been more popular due to the challenges associated with handling hydrogen gas at high pressures. However, its use to assess material behavior exposed to hydrogen gas is hindered by the difficulties intrinsic to establishing an equivalence between both charging methodologies

* Corresponding author.

E-mail address: e.martinez-paneda@imperial.ac.uk (E. Martínez-Pañeda).

<https://doi.org/10.1016/j.msea.2023.144885>

Received 22 January 2023; Received in revised form 21 February 2023; Accepted 5 March 2023

Available online 9 March 2023

0921-5093/© 2023 The Author(s). Published by Elsevier B.V. This is an open access article under the CC BY license (<http://creativecommons.org/licenses/by/4.0/>).

Nomenclature

C_L	lattice hydrogen concentration
D_{eff}	effective hydrogen diffusion coefficient
da/dN	fatigue crack growth rate (FCGR)
$(da/dN)_H$	FCGR in the presence of hydrogen
$(da/dN)_{\text{noH}}$	FCGR in the absence of hydrogen
$(da/dN)_H/(da/dN)_{\text{noH}}$	FCGR acceleration factor
ΔK	stress intensity factor range
E_s	solution energy
f_{H_2}	hydrogen fugacity
p_{H_2}	External hydrogen pressure
S_0	pre-exponential lattice Sieverts' constant
σ_h	hydrostatic stress
\bar{V}_H	partial molar volume of hydrogen

[21–23]. Consequently, there is growing interest in experimental testing in hydrogen gas environments, with particular emphasis on mimicking in-service conditions, viz. high hydrogen pressures and fatigue crack growth rate experiments. There are effectively two ways of experimentally assessing the role of hydrogen gas in accelerating fatigue crack growth rates [17]:

- (i) In-situ mechanical testing in a high-pressure hydrogen gas environment. This approach is the most representative of in-service conditions, where cracking is mainly driven by external hydrogen. However, it requires the use of sophisticated testing facilities over long periods.
- (ii) Ex-situ testing in air after pre-charging the samples in hydrogen gas (internal hydrogen). This relatively simpler methodology enables controlling the pre-charging temperature to reduce the time needed to achieve a uniform hydrogen concentration throughout the sample. However, depending on the testing time and the material diffusivity, the results can be influenced by hydrogen loss.

Both approaches have been widely used in the literature (see, e.g. Refs. [24–30] and Refs. therein) but, except for the work by Ogawa et al. [31] on austenitic steels, their characteristics and outputs have not been compared. Thus, one objective of this paper is to combine in-situ and ex-situ experimental testing with finite element analysis to shed light on the similarities and differences between these two testing approaches and understand the role of relevant testing variables (frequency, temperature, stress intensity factor range, load ratio). This study is carried out, for the first time, on ferritic CrMo steels, which display hydrogen diffusivities orders of magnitude greater than austenitic steels and are thus expected to exhibit a higher sensitivity to the testing method.

The second objective of this work is to investigate the susceptibility of base metal and heat affected zone (HAZ) microstructures to hydrogen-assisted fatigue crack growth. For both base metal and HAZ, fatigue crack growth rates have been reported to increase for smaller loading frequencies and increasing H_2 pressure and load ratio [32–35]. However, reliable in-situ fatigue crack growth rate (FCGR) data for HAZ and (particularly) coarse-grained HAZ (CGHAZ) microstructures is rather limited due to the great difficulty of testing these small areas independently [36,37]. To tackle this obstacle, suitable heat treatments are conducted on 42CrMo4 steel to produce standardised Compact-Tension (CT) samples with a coarse microstructure similar to the one that develops in the CGHAZ region of a weld. In-situ and ex-situ fatigue crack growth rate experiments are conducted under different conditions to understand the complex interactions between hydrogen uptake and diffusion, steel microstructure and testing variables. In addition, microstructural analysis and coupled finite element modelling are

conducted to interpret the results and provide a mechanistic rationale to the differences between: (i) the material behavior in CGHAZ and base metal regions, and (ii) the two testing methodologies (ex-situ vs in-situ hydrogen charging).

2. Experimental methods

2.1. Steel, heat treatments and properties

A commercial 42CrMo4 (0.42%C-0.98%Cr-0.22%Mo) steel was used. $250 \times 250 \times 12 \text{ mm}^3$ hot rolled plates were austenitized at 845°C for 40 min, quenched in water and tempered at 700°C for 2 h (base steel, BS). Then, a weld bead was deposited onto the same plate from a carbon steel wire by applying a heat input of $\sim 2 \text{ kJ/mm}$. After a thorough micro-mechanical characterization of the weld, the coarse grain heat-affected zone (CGHAZ) was identified as potentially sensitive to HE due to the coarse and more brittle microstructure that originated during cooling [32]. However, the CGHAZ is a very narrow zone, difficult to characterize independently in terms of fracture toughness, fatigue crack growth rate and hydrogen resistance, so its microstructure was reproduced in large coupons by means of a thermal treatment consisting of austenitizing at 1200°C for 20 min and quenching in oil [38,39]. Then, it was submitted to the same tempering treatment as the BS, 700°C for 2 h. This procedure allowed to manufacture standard-size CT specimens with a coarse microstructure similar to the one developed in the CGHAZ of a weld, and thus the characterization of the fatigue behavior of the CGHAZ in presence of hydrogen.

The microstructure of both grades was tempered martensite with profuse carbide precipitation being the prior austenitic grain size (PAGS) the only perceptible difference between them. Fig. 1 shows the microstructure of the as-quenched condition of the BS and the CGHAZ, where some grains have been marked for better visualization of the PAGS. While the BS has a fine microstructure with a PAGS of approximately $20 \mu\text{m}$, a coarser microstructure, with PAGS between 100 and $150 \mu\text{m}$, was measured in the CGHAZ. A similar increase in martensite lath and packet sizes was also observed.

The hardness (HV30), PAGS and mechanical properties (yield strength, σ_{ys} , ultimate tensile strength, σ_{ut} , elongation, ϵ) of the BS and CGHAZ, determined in previous works [38–40], are summarized in Table 1. Although the tensile properties of both grades are rather comparable, with less than 7% difference between them, it is interesting to note the lower fracture toughness ($J_{0.2/\text{BL}}$) displayed by the CG steel (lower than 15%), mainly due to its coarser microstructure.

The effective hydrogen diffusion coefficient (D_{eff}) of both grades, also displayed in Table 1, was obtained in previous works by fitting the desorption curve at RT of hydrogen pre-charged samples [38–40]. It is observed that an increase of the PAGS provoked a drop in D_{eff} of almost 50%, which can also be attributed to the higher hardness of this microstructure (i.e., higher dislocation density and thus a higher density of hydrogen traps [41,42]).

2.2. Fatigue crack growth tests

The influence of hydrogen on the fatigue behavior of 42CrMo4 steel welds (BS and CGHAZ) was assessed by means of FCGR tests performed (i) in air, using hydrogen pre-charged samples and (ii) in a high-pressure hydrogen gas environment. A schematic representation of both testing procedures is represented in Fig. 2.

- (i) Fatigue tests on hydrogen pre-charged samples (ex-situ tests)

Ex-situ FCGR tests were performed using standard CT specimens with a width of 48 mm and a thickness of 10 mm. Before the hydrogen charging step, the specimens were fatigue pre-cracked in air at a load ratio (R) of 0.1 and a frequency (f) of 10 Hz up to achieving an initial crack length $a_0 = 7 \text{ mm}$ ($a/W = 0.15$), following the ASTM E647

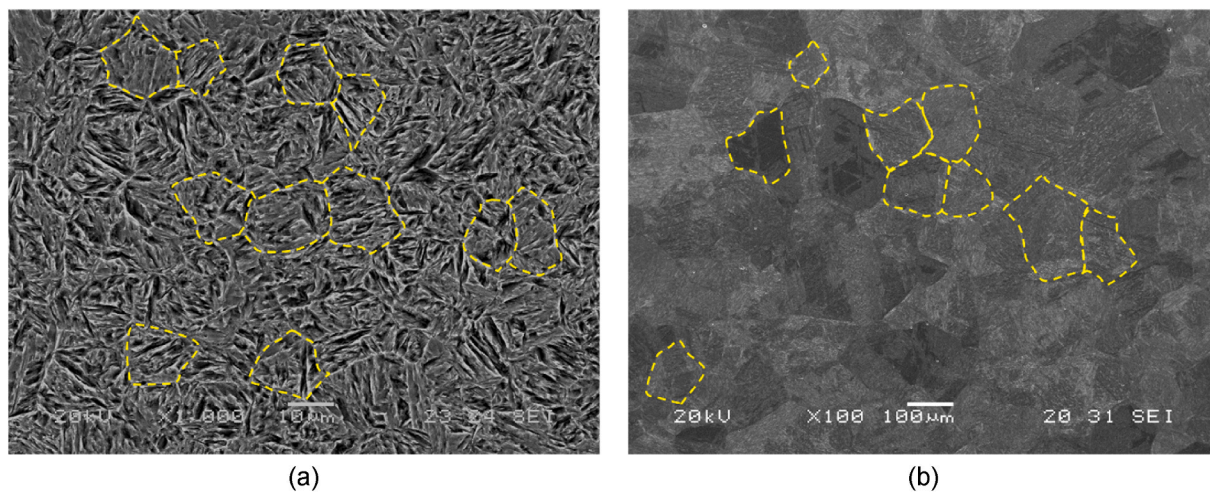


Fig. 1. Microstructure of the as-quenched (a) BS (x1000) and (b) simulated CGHAZ (x100) of 42CrMo4 steel. Some grains have been highlighted for better visualization.

Table 1
Hardness, PAGS, diffusivity and tensile properties of the BS and the CGHAZ [38–40].

Steel Grade	HV30	PAGS (μm)	D_{eff} (m ² /s)	σ_{ys} (MPa)	σ_{ut} (MPa)	e (%)	$J_{0.2/BL}$ [kJ/m ²]
BS	207	20	4.3×10^{-10}	622	710	22.6	580
CGHAZ	230	100–150	2.5×10^{-10}	600	750	23.6	488

standard [43]. The specimens were then pre-charged with hydrogen for 21 h (until saturation) in a high-pressure reactor at 450°C and at 19.5 MPa of pure gaseous hydrogen. After cooling and extracting the specimens from the reactor, the FCGR was determined in air at RT using a servohydraulic universal MTS testing machine (250 kN). The procedure is shown in Fig. 2. A cyclic load was applied from an initial stress intensity factor range (ΔK_0) of 30–35 MPa \sqrt{m} . In the course of the FCG test, the crack length was continuously monitored by means of a CTOD extensometer, allowing the representation of da/dN vs. ΔK curves. The initial and final crack lengths were measured on the fracture surface of the broken specimen, and the measured ΔK values were accordingly corrected.

Uncharged specimens were also tested at R = 0.1 under a frequency of 10 Hz. Lower frequencies have been reported to be detrimental to fatigue crack growth behavior in presence of hydrogen [26,27], so

hydrogen pre-charged specimens were tested at R = 0.1 and frequencies of 1 and 0.1 Hz.

(ii) Fatigue tests in a 35 MPa hydrogen gas atmosphere (in-situ tests)

In-situ FCGR tests were conducted at RT and 35 MPa of pure gaseous hydrogen in the *Hycomat* test bench developed by Pprime Institute at Poitiers, France. This pressure was chosen because it has been reported to be the pressure at which many hydrogen vessels should operate [44]. As shown in Fig. 2, the in-situ testing facility consists of a high-pressure autoclave assembled to a servo-hydraulic testing machine. The maximum operation pressure and temperature are 40 MPa and 150°C, respectively. For more details about the testing facility the reader is referred to Ref. [28]. In order to meet the dimensional requirements of the equipment, the CT specimens had a width of 40 mm and a thickness

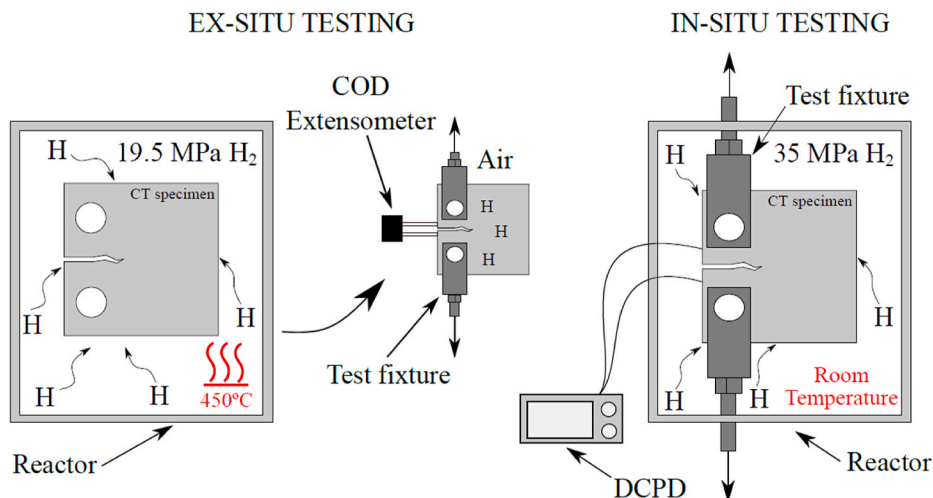


Fig. 2. Schematic representation of the ex-situ and in-situ fatigue testing methodology employed in this work.

of 10 mm. As done for the ex-situ tests, the specimens were fatigue pre-cracked in air ($R = 0.1$ and 10 Hz) until an initial crack length of $a_0 = 7$ mm ($a/W = 0.17$).

The in-situ FCGR tests were performed under load control from $\Delta K_0 \approx 30$ MPa $\sqrt{\text{m}}$ at $R = 0.1$ and frequencies of 1 and 0.1 Hz, the same conditions as for the ex-situ experiments. The crack length was measured by both optical microscopy and DCPD during the duration of the tests. As in the in-situ tests, the initial and final crack lengths were measured on the fracture surfaces of the broken specimens so as to correct the measured ΔK values.

2.3. Fracture surface observation

After the completion of the FCGR tests, the CT specimens were tensile broken and carefully cut and cleaned. In order to identify the operative fracture micromechanisms, the fracture surfaces of all the tested specimens were observed under different magnifications in a JEOL-JSM5600 scanning electron microscope under 20 kV.

3. Results

3.1. Hydrogen pre-charged specimens

3.1.1. Hydrogen concentration

For gaseous charging, the material solubility is given by Sievert's law: $S = C_L / \sqrt{f_{H_2}}$, where f_{H_2} is the fugacity of hydrogen gas and C_L is the lattice hydrogen concentration. At high temperatures and pressures, the theoretical solubility of a quenched and high-temperature tempered 42CrMo4 steel can be approximated considering Sievert's law and considering the equilibrium lattice hydrogen content of BCC iron [45], since the amount of trapped hydrogen is negligible at very high temperatures:

$$C_L = S_0 \exp\left(\frac{-E_s}{RT}\right) \sqrt{f_{H_2}} \quad (1)$$

where $S_0 = 104.47$ mol $H_2/(m^3 \sqrt{\text{MPa}})$ is the pre-exponential lattice Sieverts' constant, $E_s = 28,600$ J/mol is the solution energy, $R = 8.314$ J/(mol K) is the universal gas constant, and T is the absolute temperature (in K). The hydrogen gas fugacity (in MPa) can be related to the external pressure, p_{H_2} , as follows [46]:

$$f_{H_2} = p_{H_2} \exp\left(\frac{b p_{H_2}}{RT}\right) \quad (2)$$

where b is a constant equal to 15.84 when p_{H_2} is expressed in MPa. Applying these equations to the aforementioned hydrogen charging conditions (450°C and 19.5 MPa), a C_L of 4.1 wppm is estimated to have been introduced into the 42CrMo4 steel samples during pre-charging. However, after charging the specimens for 21 h, a cooling phase of 1 h (until reaching 85°C) was always necessary for their extraction from the reactor. Although the hydrogen pressure was maintained at 19.5 MPa during the entire cooling phase, the decrease in temperature creates a thermodynamic driving force for hydrogen egress from the specimens, which leads to significant hydrogen loss. As detailed in previous works [38,39], a total (diffusible + irreversibly trapped) hydrogen content of around 1–1.2 wppm (for both the BS and the CGHAZ) was measured in cylindrical specimens ($\varnothing = 10$ mm) using thermal desorption analysis. Finite element analysis of mass transport reveals that a total hydrogen content of ~ 1.8 wppm was present in the CT specimens at the beginning of the fatigue crack growth tests. This value lies slightly above the typical range of hydrogen absorbed by pipeline and pressure vessel steels under normal operation conditions during its service life [47].

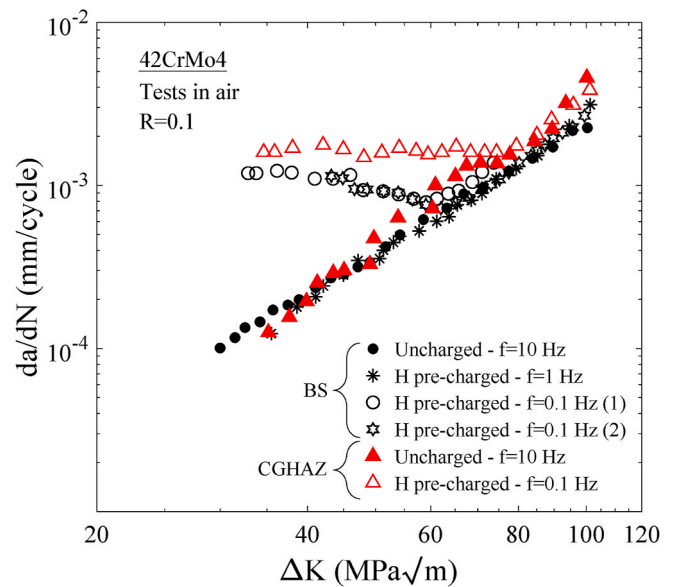


Fig. 3. Fatigue crack growth rate curves of BS and CGHAZ tested at $R = 0.1$ in air: uncharged and hydrogen pre-charged conditions. Two experiments were performed at $f = 0.1$ Hz for BS, confirming test repeatability.

3.1.2. Fatigue crack growth tests and fracture micromechanisms

The fatigue crack growth rate curves (da/dN vs. ΔK) for uncharged and hydrogen pre-charged CT specimens corresponding to the BS and the CGHAZ weld regions are shown in Fig. 3.

Consider first the results obtained with uncharged specimens. The data reveals that BS and CGHAZ display very similar FCGR behavior until intermediate ΔK values. However, from a ΔK of approximately 60 MPa $\sqrt{\text{m}}$, the crack growth rate becomes about 1.5 times higher in the CGHAZ than in the BS. This is reflected in the operative failure micromechanisms observed in the fracture surfaces of broken specimens, shown in Fig. 4. In the case of the BS, a ductile fracture micromechanism is observed along the entire crack extension. As an example, Fig. 4(a and b) shows for $\Delta K \approx 35$ MPa $\sqrt{\text{m}}$ substantial signs of plastic tearing and striation marks perpendicular to the fatigue crack propagation direction (as highlighted with yellow arrows). Regarding the CGHAZ, although a similar ductile behavior was also noticed until approximately 60 MPa $\sqrt{\text{m}}$, the overall fracture micromechanism observed for higher ΔK values is more brittle, which is exemplified in Fig. 4(c) for $\Delta K \approx 80$ MPa $\sqrt{\text{m}}$. In any case, even at these high ΔK levels, significant plasticity can also be appreciated, as evidenced by the existence of striation marks, see Fig. 4(d). This behavior was previously observed by Vargas-Arista et al. [48] in the HAZ of a 42CrMo4 steel with different grain sizes and yield strengths.

Consider now the hydrogen pre-charged specimens. First, experiments conducted on BS samples at 1 Hz showed a fatigue crack growth curve that overlaps with that of uncharged specimens, while fatigue crack growth rates increase by one order of magnitude if the loading frequency is reduced to 0.1 Hz. This sensitivity of FCGR behavior to loading frequency is well-documented and has been adequately rationalized [49,50]. If the loading frequency is sufficiently large, then there is not enough time for the hydrogen to accumulate in the fracture process zone and as a result the critical hydrogen content for embrittlement is not attained. The micrographs were consistent with this description, with striation marks (ductile fracture indicators) being clearly visible on the fracture surface of the 1 Hz samples. Since the focus here is on the embrittlement behavior, the experiments on pre-charged samples of the CGHAZ were conducted at 0.1 Hz.

For both BS and CGHAZ samples, the experiments conducted at 0.1 Hz show that, for low and medium ΔK values, an initial hydrogen content of ~ 1.8 wppm is sufficient to increase fatigue crack growth rates

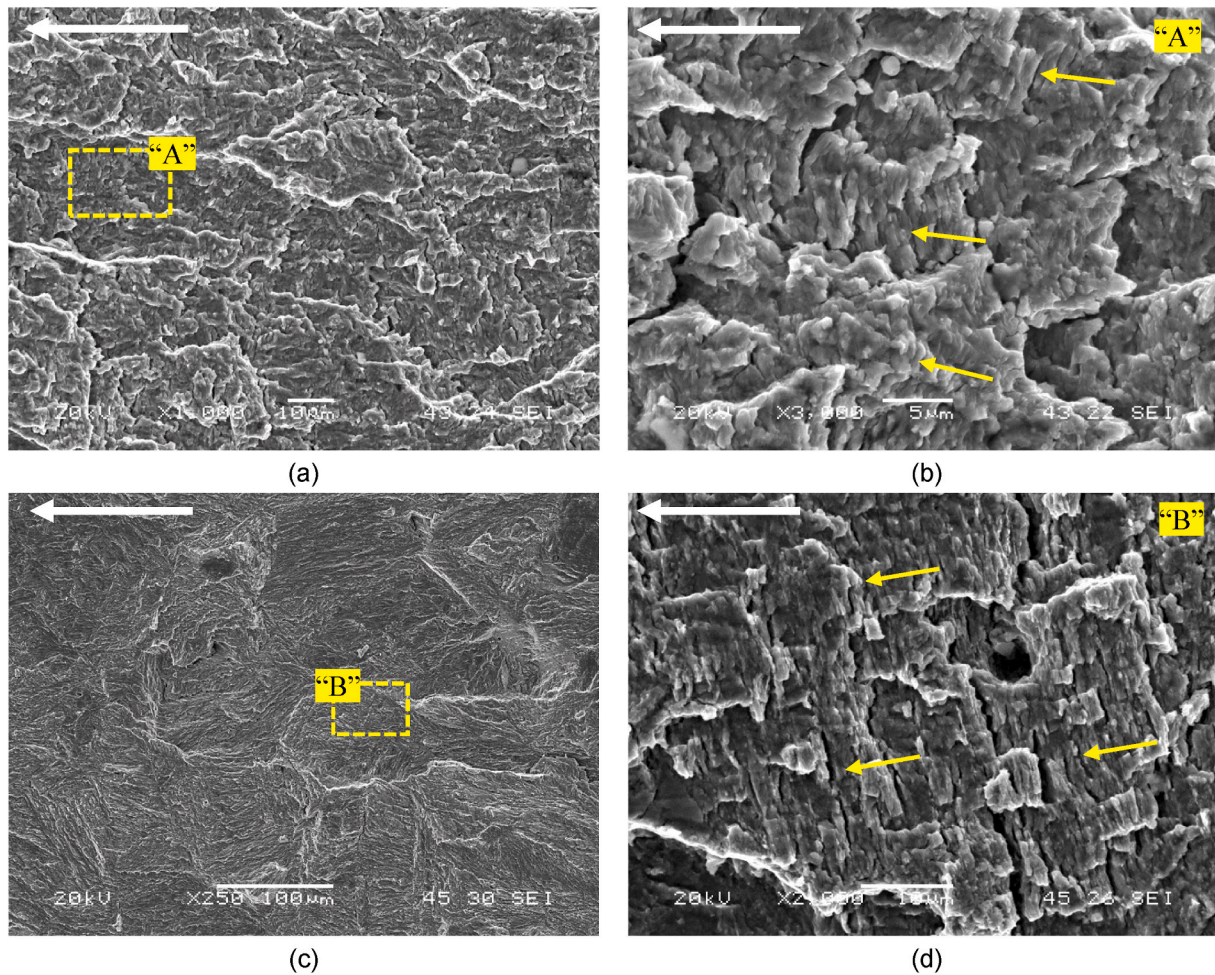


Fig. 4. SEM fracture surfaces of hydrogen uncharged specimens ($R = 0.1$ and $f = 10$ Hz) of (a, b) BS at $\Delta K \approx 35 \text{ MPa } \sqrt{\text{m}}$ and (c, d) CGHAZ at $\Delta K \approx 80 \text{ MPa } \sqrt{\text{m}}$. The white arrow shows the crack propagation direction.

by roughly one order of magnitude, relative to the hydrogen-free samples. It is also interesting to mention that under this frequency, da/dN remains practically constant from the beginning of the test ($\Delta K \approx 30\text{--}35 \text{ MPa } \sqrt{\text{m}}$) up to a ΔK value of approximately $60\text{--}70 \text{ MPa } \sqrt{\text{m}}$, when the curves converge with that of the uncharged specimens after

approximately 30 h of testing. The existence of this *plateau* region, also observed by other authors [27], is discussed below. The BS samples pre-charged with hydrogen and tested at 0.1 Hz, Fig. 5, no longer show striation marks, a clear indication of limited plastic deformation during the fracture process [51]. Other authors have also associated the absence of fatigue striations on the fracture surface with the presence of internal

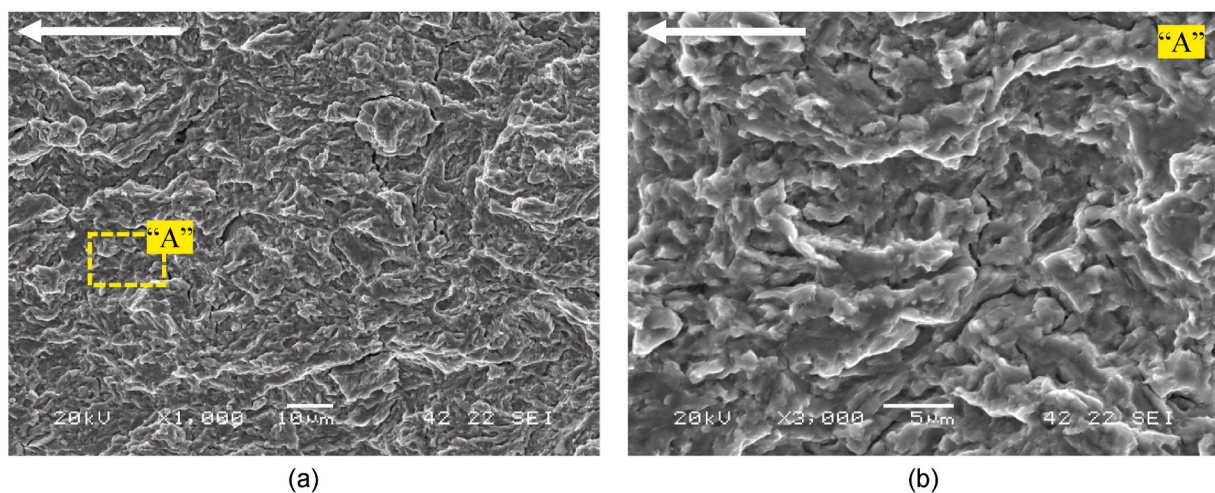


Fig. 5. SEM fracture surface at $\Delta K \approx 35 \text{ MPa } \sqrt{\text{m}}$ of hydrogen pre-charged specimens of the BS tested at $R = 0.1$ and $f = 0.1$ Hz. (a) General view at 1000x and (b) detail at 3000x. The white arrow shows the crack propagation direction.

hydrogen in fatigued specimens [52,53]. Indeed, hydrogen-assisted quasi-cleavage, already described for a wide variety of hydrogen-microstructure systems [54–56], is now the operative fracture micromechanism. In tempered martensitic steels tested in presence of hydrogen, quasi-cleavage fracture is related to the decrease of the cohesive strength of martensitic lath interfaces due to locally accumulated hydrogen [57–59]. Therefore, in this paper, this mechanism will be referred to as martensitic lath decohesion (MLD). A change in fracture micromechanisms is also observed for the hydrogen pre-charged CGHAZ samples. However, as shown in Fig. 6, the fracture surfaces of the CGHAZ are characterized by a combination of two decohesion mechanisms, MLD and intergranular (IG) fracture.

The occurrence of lath or prior austenite boundaries decohesion depends on both the local stress and local hydrogen accumulation in these interfaces, being the latter associated with dislocation slip and therefore hydrogen transport. IG failure will take place when slip systems intersect the prior austenite grain boundaries and MLD when they intersect the lath boundaries [60]. Secondary cracking is also observed along the prior austenite grain boundaries of the CGHAZ (as highlighted with yellow arrows), which is attributed to a high localized hydrogen concentration at these interfaces located ahead of the primary crack, where hydrostatic tensile stress is maximum. Other authors also suggest that secondary cracking in martensitic steels can be triggered by hydrogen-induced deformation twins impinging on grain boundaries [61]. It is worth noting the clean facets of the fractured prior austenitic grains as well as the presence of extensive flat regions, such as the one shown in Fig. 6(b), which are indicative of a lack of plastic deformation.

3.2. Specimens tested in-situ at 35 MPa hydrogen gas

3.2.1. Hydrogen concentration

The CT specimens tested in-situ were mechanically tested while being exposed to 35 MPa of pure hydrogen gas at room temperature. The application of Eqs. (1) and (2) to these testing conditions yields a C_L value of 0.006 wppm. However, at low temperatures, hydrogen trapping in different microstructural features becomes more relevant [62]. Tempered martensitic steels have a high density of structural defects (such as dislocations, martensite lath interfaces, prior austenite grain boundaries) that can sequester hydrogen at room temperature, such that the trapped hydrogen concentration can be significantly higher than the lattice one. This has been reported by several authors for low-alloy steels. For example, Yamabe et al. [63] measured the hydrogen content of a CrMo steel (0.34%C-1.04%Cr-0.20%Mo) after various exposure times to hydrogen gas at 100 MPa and RT and reported values around 0.5 wppm after 300 h. Using the same charging time and pressure but a temperature of 85°C, Macadre et al. [24] introduced a maximum of 0.3 wppm in a 40NiCrMo6 steel. Recently, Trautmann et al. [64] reported hydrogen uptake in 42CrMo4 steel of 0.15 wppm after 30 days of charging at 10 MPa and 25°C. Importantly, these measurements were performed on unloaded samples but the uptake of hydrogen can increase dramatically ahead of crack tips and other stress concentrators due to the solubility dependence on the hydrostatic stress and the increase in dislocation density [65–67].

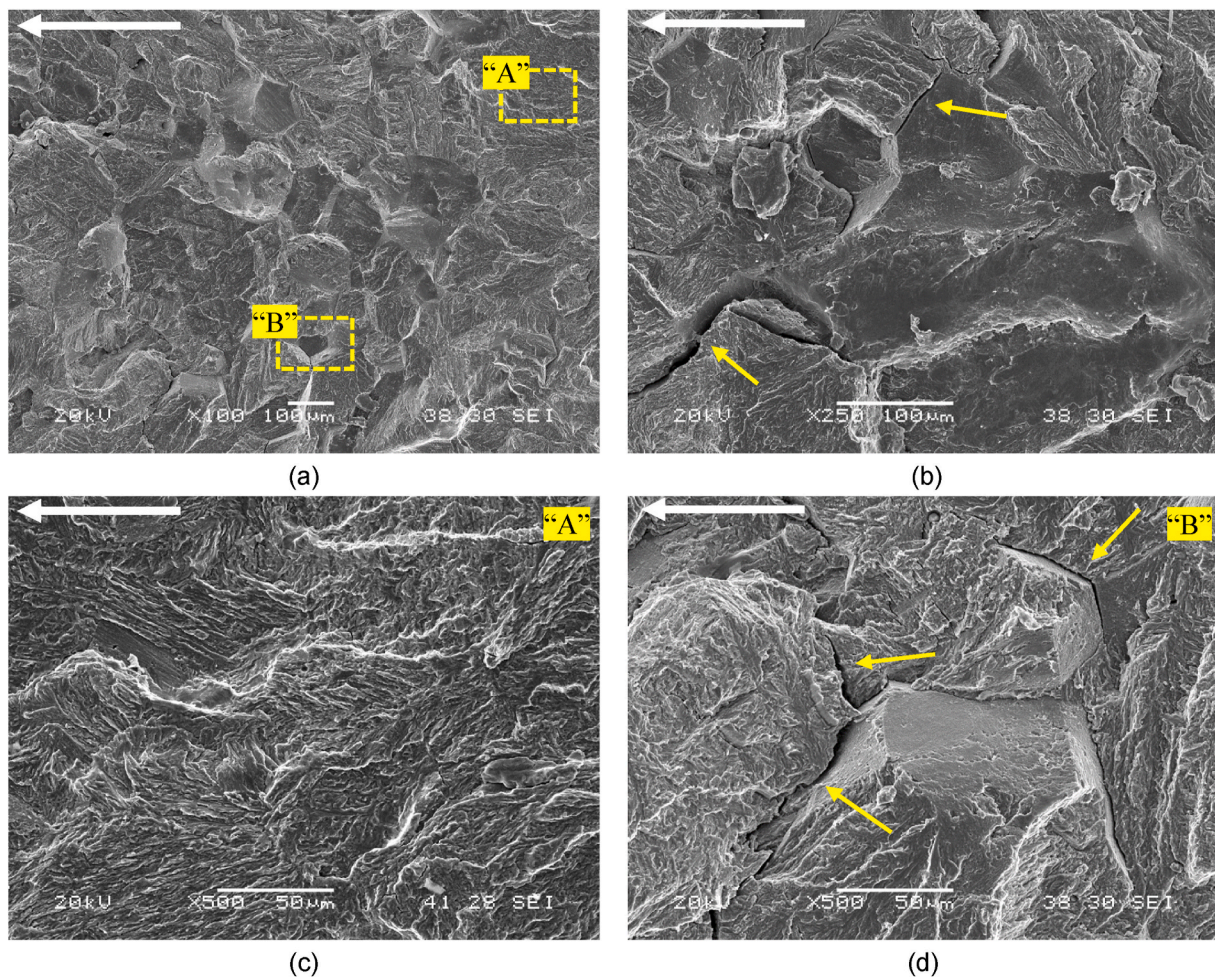


Fig. 6. SEM fracture surface at $\Delta K \approx 45 \text{ MPa} \sqrt{\text{m}}$ of hydrogen pre-charged specimens of the CGHAZ tested at $R = 0.1$ and $f = 0.1 \text{ Hz}$. (a, b) General views at 100x and 250x and (c, d) details at 500x. The white arrow shows the crack propagation direction.

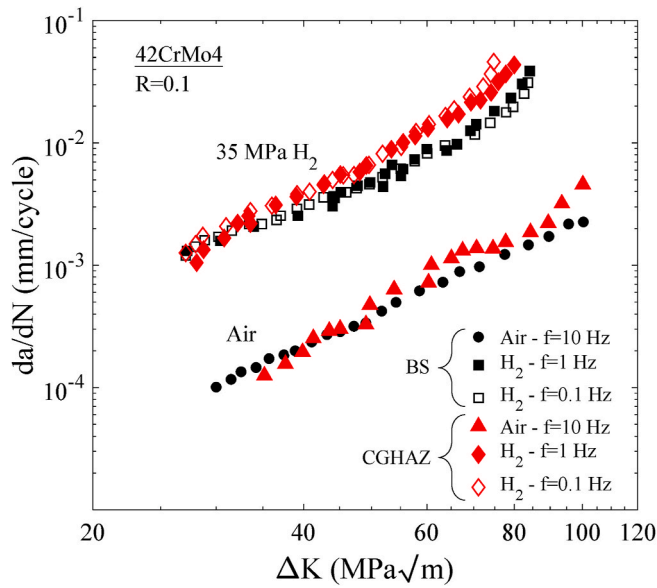


Fig. 7. Fatigue crack growth rate curves of the BS and CGHAZ tested at $R = 0.1$ in a hydrogen gas environment (with 35 MPa pressure) and in air.

3.2.2. Fatigue crack growth results and fracture micromechanisms

Fig. 7 shows the da/dN vs. ΔK curves of BS and CGHAZ specimens tested at $R = 0.1$ in air (uncharged) and in 35 MPa of pure hydrogen.

A remarkable increase of the FCGR – between 12 and 20 times - due to the presence of an external 35 MPa hydrogen atmosphere was observed in both the BS and CGHAZ. In contrast to the behavior observed in pre-charged specimens (Fig. 3), the role of hydrogen in accelerating FCGR is observed for all values of ΔK considered and for all loading frequencies (0.1 and 1 Hz). In fact, the results show very little (if any) sensitivity to the loading frequency, with the 0.1 and 1 Hz curves largely overlapping. These observations are, in general, in agreement with the literature [14,68–70]. For example, Priest [69] and Stewart [70] reported only minor differences in the FCGR curves of some CMn, CrMo and NiCrMoV steels tested in hydrogen gas between 4 and 40 MPa

when varying the frequency between 1 and 0.01 Hz. While hydrogen-assisted fatigue is known to be sensitive to the loading frequency, this sensitivity is smaller for in-situ testing and is only observed within a range of loading frequencies.

The estimated FCGR acceleration factors (ratio of da/dN in an H_2 environment, $(da/dN)_H$, to da/dN in hydrogen-free samples, $(da/dN)_{NoH}$) are shown in Fig. 8 as a function of the hydrogen gas pressure, together with literature data for (Ni)CrMo medium-strength steels [26, 38,42–44,52,91] and API X-grade pipeline steels ($400 < \sigma_{ys} < 700$ MPa) [44,71–74]. The data collected for (Ni)CrMo medium-strength steels (for $0.1 \leq f \leq 1$ Hz) is divided into two regions based on the loading ratio employed; one region where the same loading ratio as this work is employed ($R = 0.1$, region shaded in dark green) and one region with results for R between 0.3 and 0.5 (light green). The data for API X-grade pipeline steels were obtained for R values of 0.1 (dark blue points) and 0.5 (light blue points) and a loading frequency of 1 Hz. This comparison shows that the present results lie within the trend described by existing data on (Ni)CrMo medium-strength steels. Fig. 8 reveals that, in (Ni)CrMo steels, the FCGR acceleration factor increases notably with the applied pressure up to values of around 20 MPa, above which the sensitivity is lower. This is in contrast with the global behavior observed for API X-grade pipeline steels, where the fatigue acceleration factor is typically less sensitive to the hydrogen pressure, although some studies have shown otherwise [71,73,75]. Results variability is markedly greater in pipeline steels, which hinders the joint interpretation of data belonging to multiple independent studies. This degree of scatter might be attributed to the banded ferrite-pearlite microstructure of pipeline steels (material anisotropy), the presence of welded areas and the consideration of modern and vintage steels. Moreover, the fatigue performance of (Ni)CrMo steels at a given pressure appears to be, in general, better than the one of API X-grade pipeline steels. This information can be useful when assessing the use of the current natural gas transmission pipelines or the development of new systems for the transport of pure hydrogen at high pressures.

Let us now compare the behavior of the CGHAZ and the BS for in-situ testing at 35 MPa of hydrogen pressure. The results presented in Fig. 7 show that the FCGR curves corresponding to the CGHAZ always lie above those of the BS, being the differences between the corresponding da/dN vs. ΔK curves rather small at low ΔK values ($30\text{--}40$ MPa \sqrt{m}) but increasing progressively as the crack grows (greater ΔK values). Figs. 9 and 10 respectively show the fracture surfaces of the BS and CGHAZ tested in 35 MPa of hydrogen at 1 and 0.1 Hz. As can be observed in Fig. 9(a and b), the operative fracture mechanism in the BS was decohesion along martensitic lath interfaces (MLD), regardless of the applied frequency. Furthermore, the topography of the fracture surface was identical at different crack locations, which indicates that the applied ΔK did not play a relevant role in the hydrogen embrittlement process of the BS. Nevertheless, the situation in the CGHAZ is fairly different. The general fracture mechanism observed for the CGHAZ across the entire ΔK range and at both 1 and 0.1 Hz is a combination between MLD and IG fracture, as can be observed in Fig. 10(a and b) and Fig. 10(e), respectively. Clean grain facets are shown in these figures, resembling those observed for the ex-situ tests in Fig. 6(a) and (b), which are indicative of IG fracture. Moreover, abundant secondary cracking for high ΔK values was observed in the fracture surfaces of the CGHAZ, Fig. 10(c, d, f), which could explain the higher FCGR of the CGHAZ with respect to the BS at this ΔK level. Secondary cracks in the CGHAZ tested at 1 Hz (Fig. 10(c and d)) propagated mainly along the martensite lath interfaces while at 0.1 Hz secondary cracking seems to take place predominantly along grain boundaries (Fig. 10(f)). This observation is a result of hydrogen preferentially accumulating in lath and grain boundaries respectively [81] and can explain the final crack growth acceleration observed in these specimens.

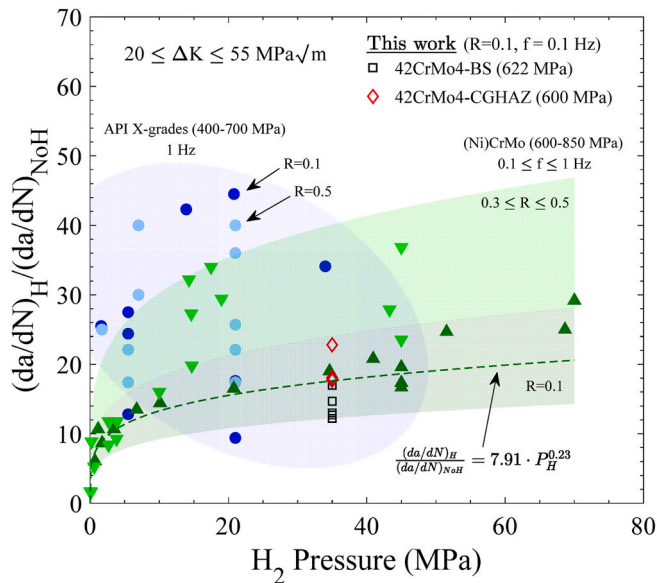


Fig. 8. Evolution of the FCGR acceleration factor with the testing H_2 pressure at ΔK between 20 and 55 MPa \sqrt{m} for a series of API X-grade pipeline steels ($400 < \sigma_{ys} < 700$ MPa) [44,71–74] and (Ni)CrMo steels ($600 < \sigma_{ys} < 850$ MPa) [14, 69,76–80]. $0.1 \leq R \leq 0.5$ and $0.1 \leq f \leq 1$ Hz.

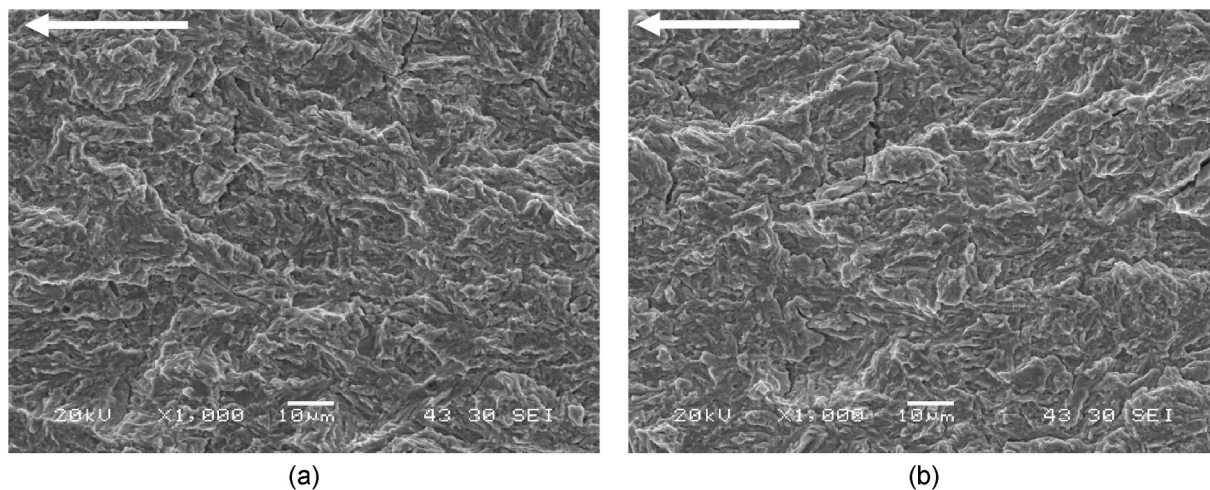


Fig. 9. SEM fracture surface at $\Delta K \approx 40 \text{ MPa} \sqrt{\text{m}}$ of BS specimens tested in 35 MPa hydrogen gas at $R = 0.1$ and (a) $f = 1 \text{ Hz}$ and (b) $f = 0.1 \text{ Hz}$. The white arrow shows the crack propagation direction.

4. Discussion

Of particular interest here is the comparison between the two testing methodologies employed to assess the influence of hydrogen on the FCGR of a 42CrMo4 steel weld: ex-situ testing using hydrogen pre-charged samples and in-situ testing in 35 MPa hydrogen gas. The effect of the frequency and ΔK will also be briefly discussed in relation to both testing approaches. Fig. 11 presents the FCGR curves ($da/dN-\Delta K$) of the BS and the CGHAZ tested at $R = 0.1$ and $f = 0.1 \text{ Hz}$ under ex-situ and in-situ conditions, as well as the reference curves obtained with uncharged specimens tested in air ($R = 0.1$ and $f = 10 \text{ Hz}$). In addition, results from the literature relevant to ferritic steels and both testing methodologies have also been added for comparison. These correspond to results from two independent sets of authors using different testing methodologies, since no works have been found that directly compare the FCGR results of ferritic steels obtained by means of in-situ and ex-situ tests. They correspond to specimens of an X65 pipeline steel ($\sigma_{ys} \approx 500 \text{ MPa}$) tested in 21 MPa hydrogen gas [74] and to electrochemically pre-charged specimens with 2 wppm of hydrogen [82], respectively.

The comparison between the pre-charged and in-situ test results obtained in this work shows significant differences despite all hydrogen FCGR curves starting at a similar level. Thus, the pre-charged samples maintain a constant da/dN at intermediate ΔK values ($da/dN = C$), while the results obtained under in-situ testing conditions exhibit the linear trend typical of stage II Paris law propagation behavior ($da/dN = C \cdot \Delta K^m$). This is observed for all tested samples. These differences are quantified in Table 2, where the values of C and m are estimated under the various testing conditions shown in Fig. 11. These results are qualitatively in line with those reported in the literature by independent works on X65 pipeline steels using pre-charged [82] and in-situ testing conditions [74]. Namely, a similar level of embrittlement is attained at the beginning of the test but the FCGR curves quickly reach a plateau for the ex-situ experiments.

The difference between in-situ and ex-situ fatigue behavior is readily appreciated in Fig. 12, where the FCGR acceleration factor is shown for both testing methodologies and both BS and CGHAZ at $R = 0.1$ and $f = 0.1 \text{ Hz}$. The results reveal that the FCGR acceleration factor is notably higher in the specimens tested in 35 MPa H_2 and essentially constant along the entire ΔK range. However, the pre-charged samples show a FCGR acceleration factor that attains a maximum value at the beginning of the test and subsequently decreases gradually until reaching a value of approximately 1 for high ΔK values (i.e., no embrittlement).

The differences between ex-situ and in-situ testing are undoubtedly

related to hydrogen uptake and re-distribution during the test. To quantify this and gain insight into the abilities of each testing methodology to characterize hydrogen assisted fatigue, coupled deformation-diffusion finite element simulations are conducted. The model employed resembles that used in Ref. [83], but restricting the focus to the lattice hydrogen distribution ahead of a stationary crack. Since the assumption of Oriani's equilibrium naturally establishes a relationship between lattice and trap occupancy, the evolution of lattice hydrogen serves to understand interfacial trap occupancy. Results are obtained for a given ΔK , using a so-called boundary layer model. Computations are performed for the BS, which has an effective diffusivity (D_{eff}) of $4.3 \times 10^{-10} \text{ m}^2/\text{s}$ (see Table 1), but the conclusions can be extrapolated to the CGHAZ. Crack tip stresses and hydrogen distributions are obtained for a frequency of 0.1 Hz, a load ratio $R = 0.1$ and a constant stress intensity factor range $\Delta K = 40 \text{ MPa} \sqrt{\text{m}}$. For the pre-charged sample, the initial lattice hydrogen concentration equals 1.02 wppm and hydrogen degassing during the test was considered by assuming a partial pressure of hydrogen in lab air equal to 0.061 Pa (equivalent to 2.7×10^{-8} wppm), which was prescribed as the boundary condition in the surface of the specimen. The hydrogen content associated with a 35 MPa H_2 environment is determined by using Sievert's law and the Noble-Able equation, incorporating the solubility dependence with the hydrostatic stress [84]:

$$C_L = S_0 \exp\left(\frac{-E_s}{RT}\right) \exp\left(\frac{\bar{V}_H \sigma_h}{RT}\right) \sqrt{f_{\text{H}_2}} \quad (3)$$

where $\bar{V}_H = 2 \times 10^{-3} \text{ m}^3/\text{mol}$ is the partial molar volume of hydrogen and σ_h is the hydrostatic stress, which is assumed to be 4 times the yield stress of the steel. Estimating with accuracy the magnitude of σ_h at the crack surface is not straightforward as small scale phenomena such as GND-hardening govern material behavior close to the crack tip; σ_h is likely to be between 2.5 and 8 times the material yield stress [66,85].

The lattice hydrogen concentrations predicted at $1 \mu\text{m}$ ahead of the crack tip, a typical critical distance for hydrogen-assisted cracking [86], are shown in Fig. 13 for both testing approaches. In both cases, and in agreement with expectations, the lattice hydrogen concentration varies cyclically due to the role that σ_h plays in driving lattice diffusion. More interestingly, it can be seen that the hydrogen concentration in the pre-charged samples quickly drops below the one relevant to the in-situ charging conditions. The rate of loss of hydrogen is greater at the beginning of the test and after a number of hours the hydrogen content near the crack tip stabilises. For the in-situ charging samples, the hydrogen concentration remains roughly constant throughout the experiment. It is worth noting that the hydrogen content in the

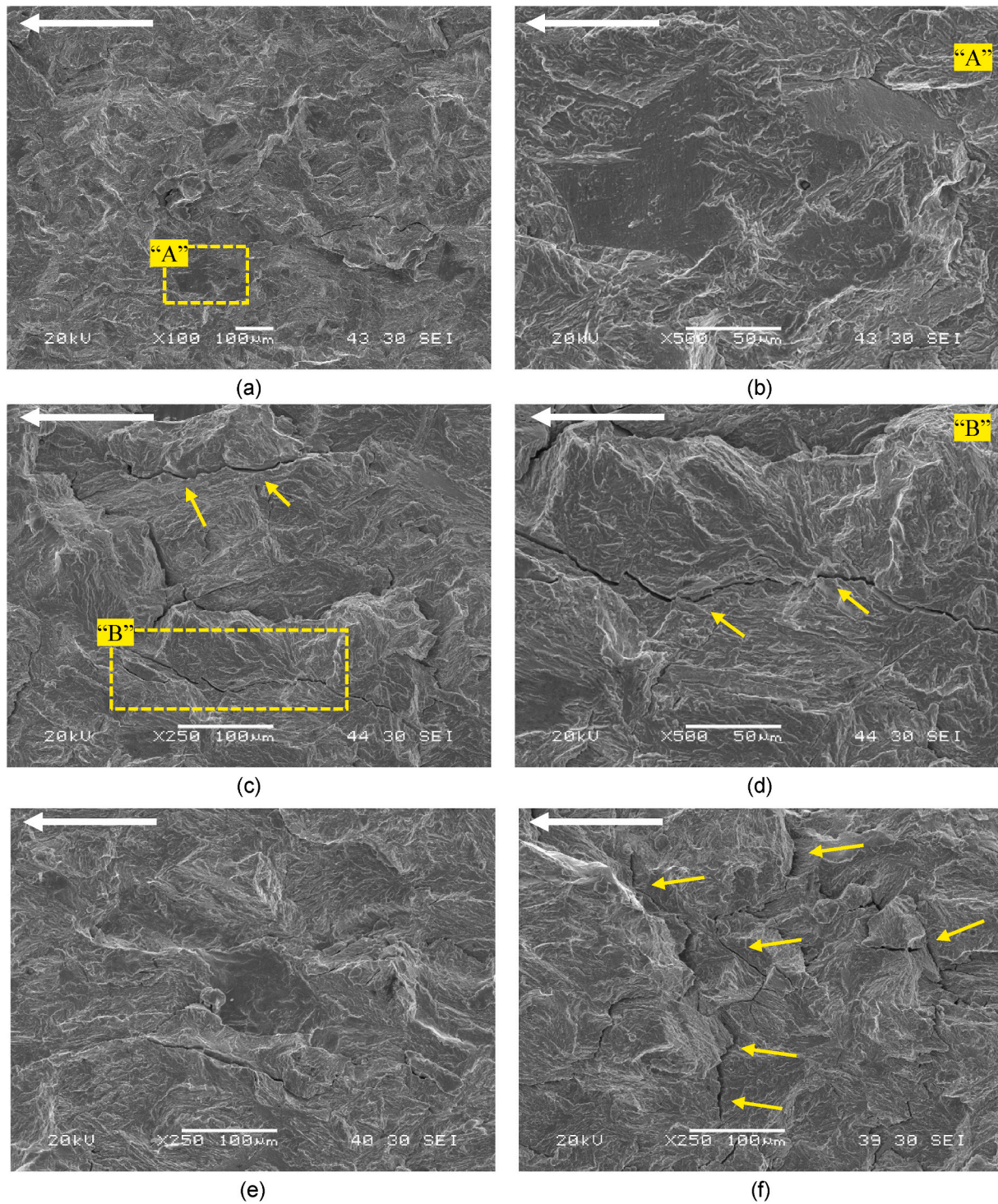


Fig. 10. SEM fracture surfaces of CGHAZ specimens tested in 35 MPa hydrogen gas at $R = 0.1$. (a, b) $f = 1$ Hz and $\Delta K = 30 \text{ MPa} \sqrt{\text{m}}$, (c, d) $f = 1$ Hz and $\Delta K \approx 60 \text{ MPa} \sqrt{\text{m}}$, (e) $f = 0.1$ Hz and $\Delta K \approx 30 \text{ MPa} \sqrt{\text{m}}$ and (f) $f = 0.1$ Hz and $\Delta K \approx 60 \text{ MPa} \sqrt{\text{m}}$. The white arrow shows the crack propagation direction.

pre-charged samples is assumed to be higher at the beginning of the experiments. This could be related to the uncertainty associated with the magnitude of σ_h at the crack surface or due to the role that the hydrogen trapped in dislocations could play in the embrittlement process through mechanisms such as the weakening of critical interfaces owing to hydrogen transfer resulting from dislocation pile ups [87]. Using this same steel, Zafra et al. [19,88] reported more than a four-fold increase in the total hydrogen concentration when a plastic pre-deformation of 50% was applied. It is thus argued that the main differences between the

testing methodologies (in-situ vs ex-situ) lie in the progressive decay of the hydrogen concentration existing in the process zone ahead of the crack during the testing in air of pre-charged specimens, in agreement with the observations made in Ref. [89]. As shown in Table 1, both the BS and CGHAZ have relatively high hydrogen diffusion coefficients, D_{eff} (2.5 and $4.3 \times 10^{-10} \text{ m}^2/\text{s}$ respectively), which according to the equation for the effective diffusivity distance ($x = 2\sqrt{D_{\text{eff}} t}$) implies that a hydrogen atom located at the center of a stress-free 10 mm-thick CT specimen would only need around 4–7 h to egress. Such hydrogen losses

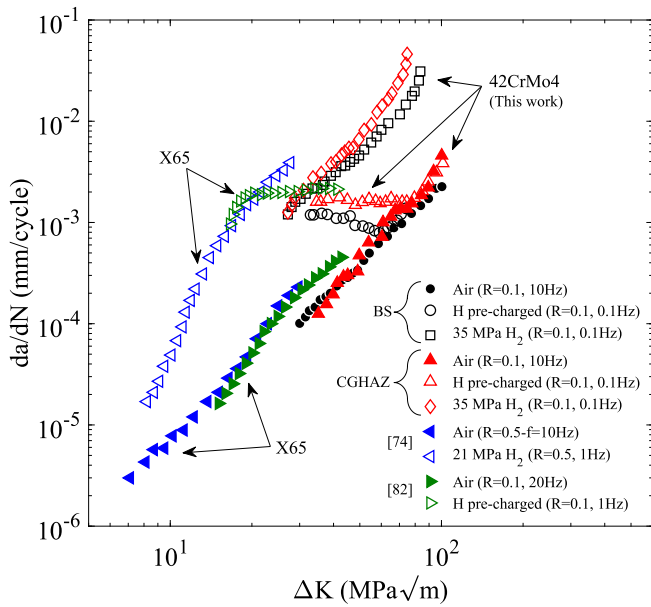


Fig. 11. Fatigue crack growth rate curves ($R = 0.1$ and $f = 0.1$ Hz) of the BS and CGHAZ of 42CrMo4 steel obtained with uncharged (air), hydrogen pre-charged (~ 1.8 wppm) and in-situ tested (35 MPa H_2) specimens. FCGR curves of X65 pipeline steel obtained in-situ (21 MPa H_2) [74] and ex-situ (pre-charged with ~ 2 wppm) [82] are included for comparison.

Table 2

Estimations of Paris law coefficients (C and m) for the materials and testing conditions considered in this work.

Grade	Testing conditions	C	m
BS	Uncharged, Air	1.55×10^{-8}	2.59
	Ex-situ	0.0012	-
	In-situ	4.24×10^{-7}	2.41
CGHAZ	Uncharged, Air	1.59×10^{-9}	3.19
	Ex-situ	0.0016	-
	In-situ	7.13×10^{-8}	2.97

could be even greater if we consider that hydrogen atoms can also escape through the crack itself. In any case, the pre-charged specimens tested in this work matched the uncharged behavior after approximately 30 h of test, which seems to indicate that hydrogen is retained in the highly stressed process zone ahead of the crack. This is confirmed in the numerical calculations given in Fig. 13 where, although slowly decreasing, a small amount of hydrogen remains in the process zone after 25 h of testing. The governing role of stress-assisted diffusion in driving hydrogen-assisted fatigue has been experimentally demonstrated using a hydrogen microprint technique [90].

Another interesting aspect is the role of the loading frequency and material diffusivity. Fernández-Sousa et al. [49] have shown that the hydrogen-assisted fatigue behavior can often be governed by the ratio between the loading frequency and the material effective diffusion coefficient. In this regard, the difference in hydrogen diffusivities between the BS and the CGHAZ could explain the higher FCGR acceleration factor observed in the CGHAZ, as its microstructure is able to retain hydrogen for longer times, increasing the amount of hydrogen that can assist fracture during every fatigue cycle. The redistribution of hydrogen within each loading cycle also rationalises the stronger influence of loading frequency in ex-situ tests, relative to the in-situ conditions. In the latter, a permanent source of hydrogen is available close to the fracture process zone while in the former the hydrogen needed to cause decohesion of internal interfaces (crack growth acceleration) must be reached by attracting hydrogen from the surroundings of the process

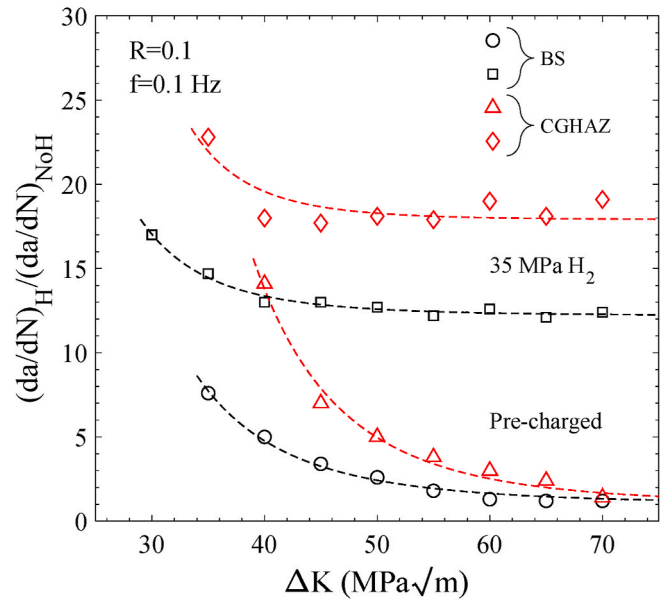


Fig. 12. Influence of the testing methodology in the evolution of the da/dN acceleration factor. Results are shown for the two materials considered (BS and CGHAZ) and the two testing conditions (pre-charged and in-situ charging at 35 MPa H_2).

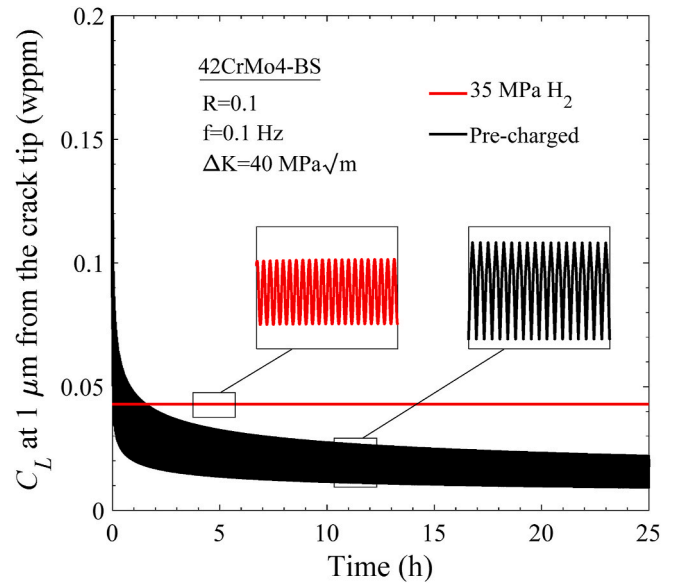


Fig. 13. Finite element predictions of lattice hydrogen concentration, C_L , at a distance $1 \mu\text{m}$ ahead of the crack tip as a function of time for both in-situ and ex-situ testing conditions. $R = 0.1$ and $f = 0.1$ Hz.

region. The smaller the loading frequency, the larger the time within each fatigue cycle that the hydrogen has to accumulate in the crack tip process zone. A reduction of frequency is associated with a decrease of the strain rate of the same order, which enhances hydrogen embrittlement [91]. However, it should be noted that the frequency dependency of hydrogen-assisted fatigue crack growth rates is not fully understood [50,92]. The combination of numerical analysis and experiments provides a mechanistic interpretation, which is graphically summarized in Fig. 14, where the sensitivity to the testing methodology and relevant testing variables (loading frequency) is exemplified.

An interesting fact to highlight is that, despite the notable differences in FCGR behavior between testing methodologies, the observed fracture

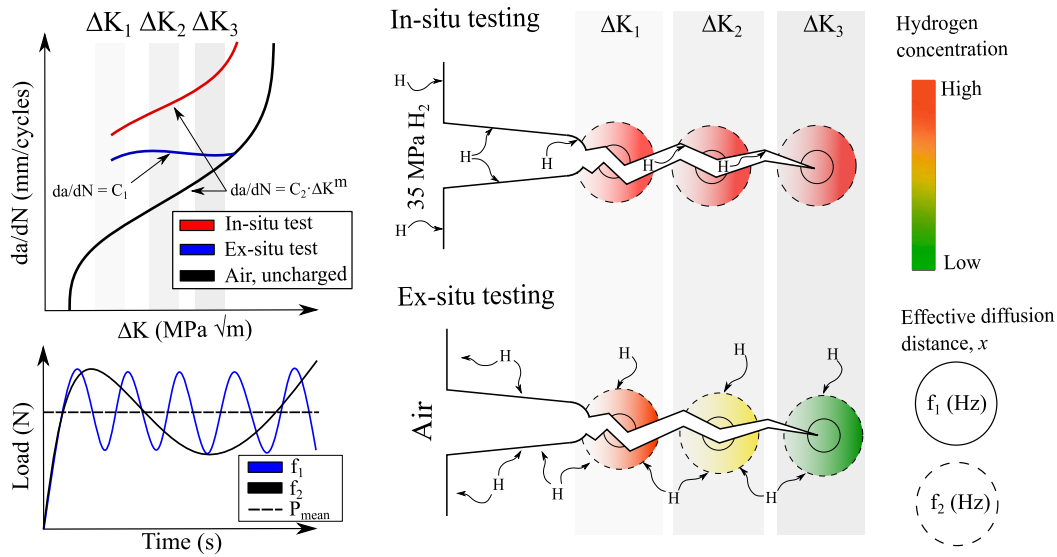


Fig. 14. Influence of the testing methodology (in-situ, ex-situ) in the hydrogen accumulation process responsible for the acceleration of the crack growth rate during fatigue tests. The figure showcases the mechanistic interpretation of the results, emphasising the hydrogen loss associated with ex-situ experiments and the role of the loading frequency, whereby lower f_2 would result in a larger time for hydrogen to accumulate.

micromechanisms were practically the same in both pre-charged and in-situ cases, as it can be observed when comparing Figs. 5 and 9 or Figs. 6 and 10. Hydrogen decohesion micromechanisms such as MLD and IG are triggered when a critical hydrogen concentration is attained in the internal interfaces present in the steel microstructure [93], which indicates the existence of a concentration threshold above which hydrogen accelerates crack growth. In this regard, it has been shown that the acceleration of the fatigue crack growth rate is considerably higher in the CGHAZ, where a combination of MLD and IG with additional secondary cracking along internal interfaces was always observed, regardless of the testing approach. Considering the rather similar mechanical properties of the BS and the CGHAZ (Table 1), which had been submitted to the same tempering treatment, this behavior can be attributed to the coarser microstructure developed in the CGHAZ.

A larger PAGS (and consequently larger martensite lath and packet sizes) is translated into a reduction of the surface per unit of volume of

prior austenite grain boundaries as well as martensite lath interfaces, which, under similar hydrogen contents (e.g., ~1.8 wppm in pre-charged samples), give rise to a higher concentration of hydrogen atoms in these interfaces. One should bear in mind that microstructural defects such as dislocations, which are important hydrogen traps, tend to accumulate in these internal interfaces, aggravating the hydrogen localizing effect. Furthermore, a finer grain size produces additional crack growth resistance since the crack has to propagate along a more tortuous path [94]. The different crack growth mechanisms observed in the BS and CGHAZ are illustrated in Fig. 15.

5. Conclusions

Fatigue crack growth rate (FCGR) experiments were conducted to compare:

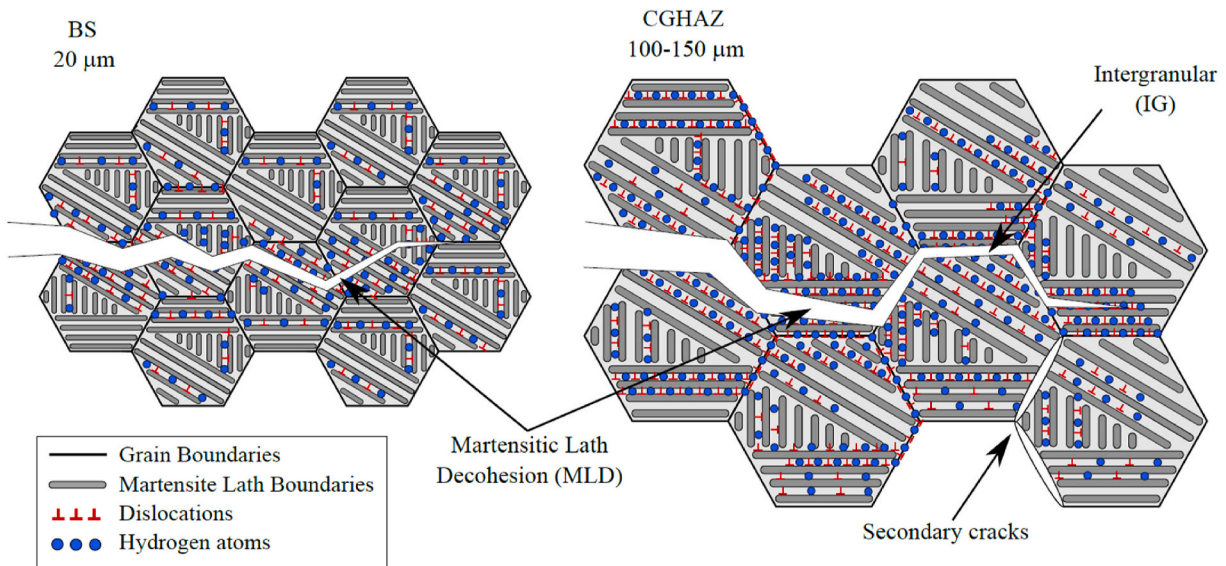


Fig. 15. Difference in crack propagation in hydrogen-containing BS and CGHAZ of 42CrMo4 steel. Accumulation of hydrogen atoms in prior austenitic grain boundaries and martensite lath boundaries.

- (i) The two approaches typically adopted to characterize material behavior in hydrogen gas – in-situ charging in an H₂ environment or hydrogen pre-charging followed by testing in air, and
- (ii) The hydrogen-assisted fatigue crack growth behavior of the two relevant regions of a 42CrMo4 steel weld – the base steel (BS) and the coarse grain heat affected zone (CGHAZ).

In addition, finite element simulations were conducted to quantify hydrogen egress during fatigue testing of pre-charged samples for the first time. This combination of experiments and numerical modelling led to the following main conclusions:

- The FCGR acceleration factor determined in BS and CGHAZ samples of 42CrMo4 steel tested at 35 MPa H₂ is always greater than in specimens pre-charged with ~1.8 wppm of hydrogen even at low ΔK values, where the hydrogen content in pre-charged specimens is highest.
- Unlike in-situ results, the FCGR curves obtained for pre-charged samples tested in air show a plateau of constant da/dN for increasing ΔK . The diminished acceleration of FCGR is shown to be the result of progressive hydrogen egress at the crack faces. Since the hydrogen content in the process zone is the result of internal hydrogen transport, a much higher sensitivity to the loading frequency is observed, relative to in-situ testing conditions.
- The presence of hydrogen in the microstructure modified the fatigue fracture micromechanisms: from ductile striation marks in hydrogen-free specimens to martensitic lath decohesion in the BS and a combination of martensite lath decohesion and intergranular fracture in the CGHAZ, with abundant secondary cracking. Interestingly, similar fracture morphologies were observed in specimens tested under in-situ and ex-situ conditions, which seems to indicate that a critical hydrogen concentration was already attained in pre-charged samples. Independent of the testing methodology, the CGHAZ showed more sensitivity to hydrogen than the BS due to its coarser microstructure.

Overall, these results and their comparison with existing literature suggest that medium-strength CrMo steels are a promising alternative for the construction of future hydrogen pipelines, especially in those cases when pressures are high and current X-grade steel pipelines cannot be safely adapted to transport pure hydrogen. Nevertheless, care should be taken when characterizing fatigue behavior in air using pre-charged samples as this provides non-conservative estimates.

CRedit authorship contribution statement

A. Zafra: Conceptualization, Methodology, Validation, Formal analysis, Investigation, Resources, Data curation, Writing – original draft, Writing – review & editing, Visualization. **G. Álvarez:** Conceptualization, Methodology, Software, Formal analysis, Investigation, Data curation, Writing – review & editing, Visualization. **G. Benoit:** Methodology, Resources, Writing – review & editing. **G. Henaff:** Methodology, Resources, Writing – review & editing. **E. Martínez-Pañeda:** Conceptualization, Methodology, Software, Resources, Writing – review & editing, Supervision, Funding acquisition. **C. Rodríguez:** Conceptualization, Writing – review & editing, Supervision, Project administration, Funding acquisition. **J. Belzunce:** Conceptualization, Writing – review & editing, Supervision, Project administration, Funding acquisition.

Declaration of competing interest

The authors declare that they have no known competing financial interests or personal relationships that could have appeared to influence the work reported in this paper.

Data availability

Data will be made available on request.

Acknowledgements

The authors would like to thank the Spanish Ministry of Science, Innovation and Universities for the financial support received to carry out research project RTI2018-096070-B-C31 (H2steelweld). A. Zafra and G. Álvarez thank the Spanish Ministry of Universities for the Margarita Salas Postdoctoral Fellowships [reference MU-21-UP2021-030] funded through the Next Generation EU programme. E. Martínez-Pañeda was additionally supported by an UKRI Future Leaders Fellowship [grant MR/V024124/1]. This work pertains to the French Government programs “Investissements d’Avenir” LABEX INTERACTIFS [reference ANR-11-LABX-0017-01]. Finally, the authors would also like to acknowledge the technical support provided by the Scientific and Technical Service of the University of Oviedo for the use of the SEM JEOLJSM5600 scanning electron microscope.

References

- [1] S.E. Hosseini, M.A. Wahid, Hydrogen production from renewable and sustainable energy resources: promising green energy carrier for clean development, *Renew. Sustain. Energy Rev.* 57 (2016) 850–866, <https://doi.org/10.1016/j.rser.2015.12.112>.
- [2] A. Nagao, C.D. Smith, M. Dadfarnia, P. Sofronis, I.M. Robertson, The role of hydrogen in hydrogen embrittlement fracture of lath martensitic steel, *Acta Mater.* 60 (2012) 5182–5189, <https://doi.org/10.1016/j.actamat.2012.06.040>.
- [3] B.P. Somerday, P. Sofronis, K.A. Nibur, C. San Marchi, R. Kirchheim, Elucidating the variables affecting accelerated fatigue crack growth of steels in hydrogen gas with low oxygen concentrations, *Acta Mater.* 61 (2013) 6153–6170, <https://doi.org/10.1016/j.actamat.2013.07.001>.
- [4] D. Guedes, L. Cupertino Malheiros, A. Oudriss, S. Cohendoz, J. Bouhattate, J. Creus, et al., The role of plasticity and hydrogen flux in the fracture of a tempered martensitic steel: a new design of mechanical test until fracture to separate the influence of mobile from deeply trapped hydrogen, *Acta Mater.* 186 (2020) 133–148, <https://doi.org/10.1016/j.actamat.2019.12.045>.
- [5] Y. Murakami, R.O. Ritchie, Effects of hydrogen on fatigue-crack propagation in steels, *Gaseous Hydrogen Embrittlement Mater. Energy Technol.: Problem, Charact. Eff. Part Alloy Cl.* (2012) 379–417, <https://doi.org/10.1533/9780857093899.2.379>.
- [6] A. Zafra, L.B. Peral, J. Belzunce, C. Rodríguez, Effects of hydrogen on the fracture toughness of 42CrMo4 steel quenched and tempered at different temperatures, *Int. J. Pres. Ves. Pip.* 171 (2019) 34–50, <https://doi.org/10.1016/j.ijpvp.2019.01.020>.
- [7] S. Pillot, L. Coudreuse, Hydrogen-induced disbonding and embrittlement of steels used in petrochemical refining, *Gaseous Hydrogen Embrittlement Mater. Energy Technol.: Problem, Charact. Eff. Part Alloy Cl.* (2012) 51–93, <https://doi.org/10.1533/9780857093899.1.51>.
- [8] M. Tvrđý, S. Havel, L. Hyspecká, K. Mazanec, Hydrogen embrittlement of CrMo and CrMoV pressure vessel steels, *Int. J. Pres. Ves. Pip.* 9 (1981) 355–365, [https://doi.org/10.1016/0308-0161\(81\)90008-9](https://doi.org/10.1016/0308-0161(81)90008-9).
- [9] J. Koutský, K. Šplíchal, Hydrogen and radiation embrittlement of CrMoV and CrNiMoV ferritic RPV steels, *Int. J. Pres. Ves. Pip.* 24 (1986) 13–26, [https://doi.org/10.1016/0308-0161\(86\)90027-X](https://doi.org/10.1016/0308-0161(86)90027-X).
- [10] K. Šplíchal, M. Ruščák, J. Žďárek, Combination of radiation and hydrogen damage of reactor pressure vessel materials, *Int. J. Pres. Ves. Pip.* 55 (1993) 361–373, [https://doi.org/10.1016/0308-0161\(93\)90057-Z](https://doi.org/10.1016/0308-0161(93)90057-Z).
- [11] J.C. Lippold, *Welding Metallurgy and Weldability*, Ohio State University: John Wiley and Sons, 2015.
- [12] M. Nagumo, *Fundamentals of Hydrogen Embrittlement*, 2016, <https://doi.org/10.1007/978-981-10-0161-1>.
- [13] C.A. Zapffe, C.E. Sims, Hydrogen embrittlement, internal stress and defects in steel, *Trans. AIME* 145 (1941) 225–261.
- [14] C. San Marchi, B.P. Somerday, Technical Reference for Hydrogen Compatibility of Materials, 2012, <https://doi.org/10.1016/j.juro.2008.04.178>. Sandia Report.
- [15] K. Xu, Hydrogen embrittlement of carbon steels and their welds, *Gaseous Hydrogen Embrittlement Mater. Energy Technol.: Problem, Charact. Eff. Part Alloy Cl.* (2012) 526–561, <https://doi.org/10.1533/9780857093899.3.526>.
- [16] G. Álvarez, A. Zafra, C. Rodríguez, F.J. Belzunce, Cuesta II, SPT analysis of hydrogen embrittlement in CrMoV welds, *Theor. Appl. Fract. Mech.* 110 (2020), <https://doi.org/10.1016/j.tafmec.2020.102813>.
- [17] R.P. Gangloff, B.P. Somerday, *Gaseous Hydrogen Embrittlement of Materials in Energy Technologies: the Problem, its Characterization and Effects on Particular Alloy Classes*, Woodhead Publishing, 2012.
- [18] G. Álvarez, A. Zafra, F.J. Belzunce, C. Rodríguez, Hydrogen embrittlement testing procedure for the analysis of structural steels with Small Punch Tests using notched specimens, *Eng. Fract. Mech.* 253 (2021) 1–14, <https://doi.org/10.1016/j.engfracmech.2021.107906>.

- [69] A.H. Priest, Fatigue Crack Growth and Fracture Resistance of Steels in High-Pressure Hydrogen Environments, 1983.
- [70] A.T. Stewart, The effect of hydrogen on fatigue crack propagation in steels, in: *Mechanisms of Environment Sensitive Cracking of Materials*, The Metals Society, 1977, pp. 400–410.
- [71] A.J. Slifka, E.S. Drexler, N.E. Nanninga, Y.S. Levy, J.D. McColskey, R.L. Amaro, et al., Fatigue crack growth of two pipeline steels in a pressurized hydrogen environment, *Corrosion Sci.* 78 (2014) 313–321, <https://doi.org/10.1016/j.corsci.2013.10.014>.
- [72] R. Zawierucha, K. Xu, Hydrogen pipeline steels, in: *Proceedings of Materials Science and Technology - Materials for the Hydrogen Economy*, MS&T, OH, 2005, pp. 79–90.
- [73] C.S. Marchi, B.P. Somerday, K.A. Nibur, D.G. Stalheim, T. Boggess, S. Jansto, Fracture and fatigue of commercial grade api pipeline steels in gaseous hydrogen, *Am. Soc. Mech. Eng. Pres. Ves. Pip. Div.* 6 (2010) 939–948, <https://doi.org/10.1115/PVP2010-25825>.
- [74] J.A. Ronevich, B.P. Somerday, C.W. San Marchi, Effects of microstructure banding on hydrogen assisted fatigue crack growth in X65 pipeline steels, *Int. J. Fatig.* 82 (2016) 497–504, <https://doi.org/10.1016/j.ijfatigue.2015.09.004>.
- [75] N. Nanninga, A. Slifka, Y. Levy, C. White, A review of fatigue crack growth for pipeline steels exposed to hydrogen, *J. Res. Natl. Inst. Stand. Technol.* 115 (2010) 437–452, <https://doi.org/10.6028/jres.115.030>.
- [76] Z. Hua, X. Zhang, J. Zheng, C. Gu, T. Cui, Y. Zhao, et al., Hydrogen-enhanced fatigue life analysis of Cr–Mo steel high-pressure vessels, *Int. J. Hydrogen Energy* 42 (2017) 12005–12014, <https://doi.org/10.1016/j.ijhydene.2017.02.103>.
- [77] R.L.S. Thomas, J.R. Scully, R.P. Gangloff, H. Shimazu, S. Konosu, Y. Tanaka, et al., Internal hydrogen embrittlement of ultrahigh-strength AERMET 100 steel, *Metall. Trans. A* 276 (2017) 1–7, <https://doi.org/10.1007/BF02647003>.
- [78] Nibur KA, Somerday BP. Pvp2010-25827 Fracture and Fatigue Tolerant Steel Pressure Vessels for 2010:1–10.
- [79] A. Macadre, M. Artamonov, S. Matsuoka, J. Furtado, Effects of hydrogen pressure and test frequency on fatigue crack growth properties of Ni–Cr–Mo steel candidate for a storage cylinder of a 70MPa hydrogen filling station, *Eng. Fract. Mech.* 78 (2011) 3196–3211, <https://doi.org/10.1016/j.engfracmech.2011.09.007>.
- [80] T. Miyamoto, T. Matsu, N. Kobayashi, Y. Mukaie, S. Matsuoka, Characteristics of fatigue life and fatigue crack growth of SCM435 steel in high-pressure hydrogen gas, *Nihon Kikai Gakkai Ronbunshu, A Hen/Trans. Jpn. Soc. Mech. Eng.* 78 (2012) 531–546, <https://doi.org/10.1299/kikaia.78.531>.
- [81] P. Gong, A. Turk, J. Nutter, F. Yu, B. Wynne, P. Rivera-Diaz-del-Castillo, et al., Hydrogen embrittlement mechanisms in advanced high strength steel, *Acta Mater.* 223 (2022), <https://doi.org/10.1016/j.actamat.2021.117488>.
- [82] Augusto Sciuccati, Mechanical Behaviour of High Toughness Steels in Extreme Environments: Influence of Hydrogen and Low Temperature, PhD thesis, Politecnico di Milano, 2011.
- [83] A. Golahmar, P.K. Kristensen, C.F. Niordson, E. Martínez-pañeda, A phase field model for hydrogen-assisted fatigue, *Int. J. Fatig.* 154 (2022), 106521, <https://doi.org/10.1016/j.ijfatigue.2021.106521>.
- [84] E. Martínez-Pañeda, A. Díaz, L. Wright, A. Turnbull, Generalised boundary conditions for hydrogen transport at crack tips, *Corrosion Sci.* 173 (2020), 108698, <https://doi.org/10.1016/j.corsci.2020.108698>.
- [85] E. Martínez-pañeda, V.S. Deshpande, C.F. Niordson, N.A. Fleck, The role of plastic strain gradients in the crack growth resistance of metals, *J. Mech. Phys. Solid.* 126 (2019) 136–150, <https://doi.org/10.1016/j.jmps.2019.02.011>.
- [86] E. Martínez-Pañeda, C.F. Niordson, R.P. Gangloff, Strain gradient plasticity-based modeling of hydrogen environment assisted cracking, *Acta Mater.* 117 (2016) 321–332, <https://doi.org/10.1016/j.actamat.2016.07.022>.
- [87] H.J. Maier, H. Kaesche, Plastic deformation: a major factor in hydrogen embrittlement of low alloy steel, *Mater. Sci. Eng.* 117 (1989), [https://doi.org/10.1016/0921-5093\(89\)90112-3](https://doi.org/10.1016/0921-5093(89)90112-3).
- [88] A. Zafra, Study on Hydrogen Diffusivity and Embrittlement of Quenched and Tempered 42CrMo4 Steel, PhD Thesis, University of Oviedo, Spain, 2021.
- [89] D. Wang, A.B. Hagen, P.U. Fathi, M. Lin, R. Johnsen, X. Lu, Investigation of hydrogen embrittlement behavior in X65 pipeline steel under different hydrogen charging conditions, *Mater. Sci. Eng.* 860 (2022), 144262, <https://doi.org/10.1016/j.msea.2022.144262>.
- [90] M. Nakatani, H. Fujihara, M. Sakihara, K. Minoshima, Fatigue crack growth acceleration caused by irreversible hydrogen desorption in high-strength steel and its mechanical condition, *Mater. Sci. Eng.* 528 (2011) 7729–7738, <https://doi.org/10.1016/j.msea.2011.07.003>.
- [91] A. Roy, I. Manna, S. Tarafder, S. Sivaprasad, S. Paswan, I. Chattoraj, Hydrogen enhanced fatigue crack growth in an HSLA steel, *Mater. Sci. Eng.* 588 (2013) 86–96, <https://doi.org/10.1016/j.msea.2013.08.079>.
- [92] H. Matsunaga, O. Takakuwa, J. Yamabe, S. Matsuoka, Hydrogen-enhanced fatigue crack growth in steels and its frequency dependence, *Phil. Trans. Math. Phys. Eng. Sci.* 375 (2017), <https://doi.org/10.1098/rsta.2016.0412>.
- [93] R.A. Oriani, A mechanistic theory of hydrogen embrittlement of steels, *Berichte der Bunsen-Gesellschaft für Physikalische Chemie* 76 (1972) 848–857.
- [94] V.R. Nagarajan, S.K. Putatunda, J. Boileau, Fatigue crack growth behavior of austempered AISI 4140 steel with dissolved hydrogen, *Metals* 7 (2017) 1–18, <https://doi.org/10.3390/met7110466>.